Precipitation behaviour of Al_3Zr precipitate in Al−Cu−Zr and Al−Cu−Zr−Ti−V alloys

JIA Zhi-hong[1,2], Jean-Philippe COUZINIÉ[3], Nadia CHERDOUDI[3], Ivan GUILLOT[3], Lars ARNBERG[2],
Petter ÅSHOLT[4], Stig BRUSETHAUG[4], Bruno BARLAS[5], Denis MASSINON[5]

1. College of Materials Science and Engineering, Chongqing University, Chongqing 400044, China;
2. Department of Materials Science and Engineering, Norwegian University of Science and Technology,
NO-7491, Trondheim, Norway;
3. Institut de Chimie et des Matériaux Paris-Est, UMR 7182 CNRS-Unversité Paris Val de Marne,
2-8 rue Henri Dunant, 94320, Thiais, France;
4. Hydro Aluminium Research and Technology Development, N-6601 Sunndalsøra,
Norway Montupet SA, 60181 Nogent sur Oise Cedex, France;
5. Mentupet SA, 60181 Nogent sur Oise Cedex, France

Abstract: The precipitation behaviours of Al_3Zr precipitate in the Al−Cu−Zr and Al−Cu−Zr−Ti−V alloys were studied by transmission electron microscopy. Metastable Al_3Zr precipitates are homogeneously nucleated in dendrite centres resulting in homogeneous distribution. However, the precipitation in the interdendritic regions is complex and the precipitation morphologies, helical-like and stripe-like shapes, were observed, which are composed of many spherical Al_3Zr precipitates. The stripe-like precipitate clusters have preferential orientations along with the $\langle 100 \rangle$ Al directions, which is inferred to be related to $\theta'(Al_2Cu)$ and θ phases. Addition of Cu can accelerate the $L1_2 \longrightarrow D0_{23}$ structural transformation of the Al_3Zr precipitate.
Key words: aluminium alloys; Al_3Zr precipitate; phase transformation

1 Introduction

The age-hardening treated Al−Cu alloys are used for structural components because of the formation of GP zones in an initial stage of ageing with subsequent precipitation of θ'' and θ' Al_2Cu phases leading to a pronounced improvement in the strength properties [1]. However, Al_2Cu hardening phase at high temperature will transform to stable phases which greatly reduce the material strength [2]. On the other hand modern combustion engines will require increased pressures and temperatures exerted upon some components. This requires the material to be able to sustain work temperature above 250 °C. A material with a microstructure containing thermally stable and coherent phase in the Al matrix is required.

The metastable Al_3Zr phase with $L1_2$ structure is a good candidate. Because of a low solubility [3] and diffusivity [4] of Zr in the Al matrix, the coherent Al_3Zr precipitate is very stable at high temperatures. Nucleation and growth of Al_3Zr precipitates have been well studied by both modelling and experimental methods [4−10]. Precipitate evolution and morphologies of Al_3Zr precipitates in Al−Zr and Al−Zr−Ti alloys have been investigated systematically [11,12]. Different morphologies of Al_3Zr and $Al_3(Zr,Ti)$ precipitates were observed particularly at dendrite edges or in interdendritic regions. The presence of other alloying elements may influence Al_3Zr precipitates in several ways. For instance, it has been predicted that the additions of Cu, Mg and Zn in commercial 7050 alloy accelerate the Al_3Zr precipitation kinetics compared with a binary Al−Zr alloys [13]. On the other hand, the addition of Ti or V to Al−Zr alloys can change the structure of Al_3Zr phase into $D0_{22}$ structure, which is

formed instead of the equilibrium $D0_{23}$ [14,15].

There are several studies of Zr additions to wrought aluminium alloys, which focus on the recrystallization resistance during heat treatment by a drag force of coherent Al_3Zr precipitate on motion [4,16−19]. The effect of Zr on cast aluminium alloys, however, has been rarely studied [1,20]. In the present work, precipitation, distribution and morphology of Al_3Zr or $Al_3(Zr,Ti,V)$ precipitates in Al−Cu cast alloys were studied to develop aluminium alloys for elevated temperature applications.

2 Experimental

Two alloys (Al−5.0%Cu−0.2%Zr and Al−5.0%Cu−0.2%Zr−0.1%Ti−0.2%V, mass fraction) were investigated. The alloy was cast by a direct chill method to cylindrical bars with a diameter of 18 mm and a length of 200 mm. As-cast specimens were heat treated at a rate of 50 °C/h up to 500 °C and kept at this temperature for 1, 5, 20 h, respectively, and subsequently water-quenched.

A JEOL 2010 transmission electron microscope (TEM) operated at 200 kV was used to investigate precipitation of Al_3Zr and $Al_3(Zr,Ti,V)$ in various variants. A double-tilt sample holder tilting up to ± 30° was used. TEM foils were prepared by mechanically grinding down to 80 μm, dimpling down to 20 μm and finally ion-milling until perforation. Precipitate radii were determined by image analyses of 40 digitized TEM micrographs using Image J software complemented with a dedicated script. High-resolution TEM images were taken by a JEOL 2010F microscope.

3 Results

Figure 1(a) shows TEM micrographs of precipitates in a large region across a dendrite to the interdendritic region in the Al−Cu−Zr−Ti−V alloy heat treated at 500 °C for 5 h. It is clear that precipitates are spherical, small and have a high density in dendrites, while they are relative big and have a low density in interdendritic region. Compositional analyses of randomly selected precipitates reveal that the precipitate is composed of Al, Zr, Ti and V. All precipitates at this treatment condition are coherent with the Al matrix as confirmed by existence of superlattice reflections in the insert diffraction pattern. Actually, the size and density of precipitates also vary from the dendritic centre to the dendrite edge. Figure 1(b) gives statistics of the size distribution of precipitates based on 40 images including 2400 precipitates taken from the dendrite centre to edge. A mean radius of the precipitate is (5.8 ± 2.0) nm.
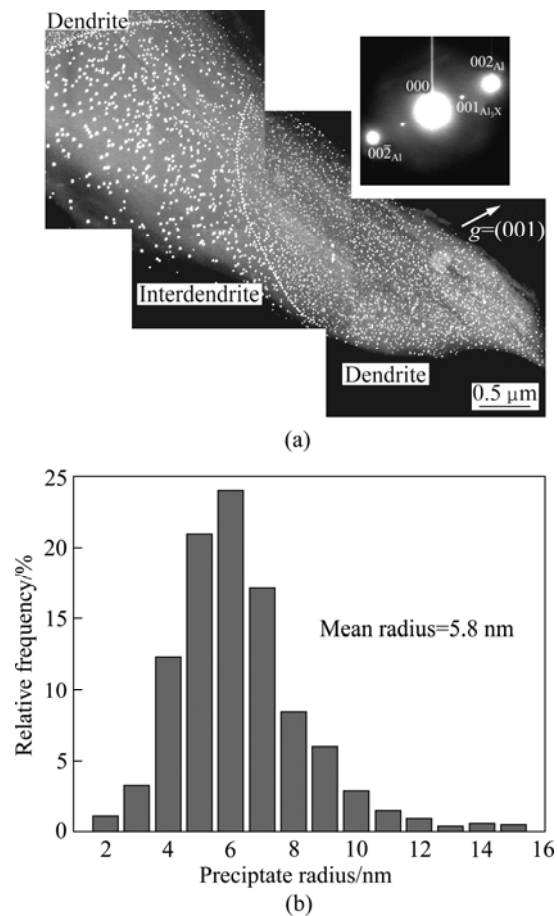
Fig. 1 TEM dark-field image (imaged with $\vec{g} = (001)$ $L1_2$ superlattice reflection) (a), precipitate size distribution obtained from TEM image taken from dendrite centre to edge (b)

Precipitation at dendrite edges or interdendritic regions was found to be complex. Figures 2(a) and (b) display two representative morphologies, named as helical-like and strip-like shapes, formed by precipitation in the Al−Cu−Zr alloy heat treated at 500 °C for 5 h. The strip-like morphology is more common. Bright-field (Fig. 2(c)) and tilting dark-field (Fig. 2(d)) images show dislocations across the precipitate region. However, sharp edges observed in strip-like morphologies indicate that precipitation of Al_3Zr precipitates is not completely related to dislocations. In addition, precipitate-free zone was also observed in the interdendritic regions (Figs. 2(a) and b).

TEM investigations along low-index zone axes were done. Figure 3(a) shows a TEM dark-field image take from [001] direction in an interdendritic region. Precipitation of particles following straight lines along two ⟨100⟩ perpendicular directions of the Al matrix can be observed. Figure 3(b) was taken from the same area as Fig. 3(a), but at about 30° tilting. This reveals that the precipitates lie on a plane. Precipitation preferentially begins in the Al (001) and (010) planes.
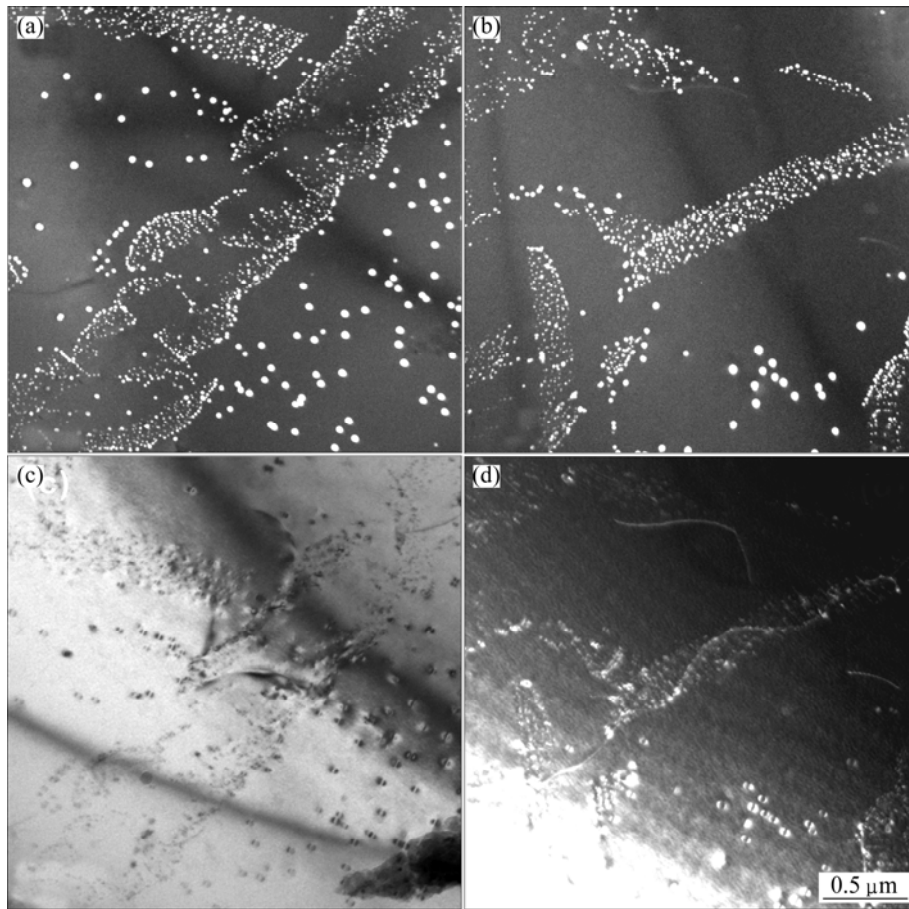
Fig. 2 TEM images taken from interdendritic regions showing complex morphologies of precipitation of Al$_3$Zr precipitates: (a, b) Dark-field images from two different regions of Al−Cu−Zr alloy; (c) Bright-field image of (a); (d) Dark-field image from same area as (b) but slightly tilting relative to (c) orientation (Dislocations were observed in (c) and (d))
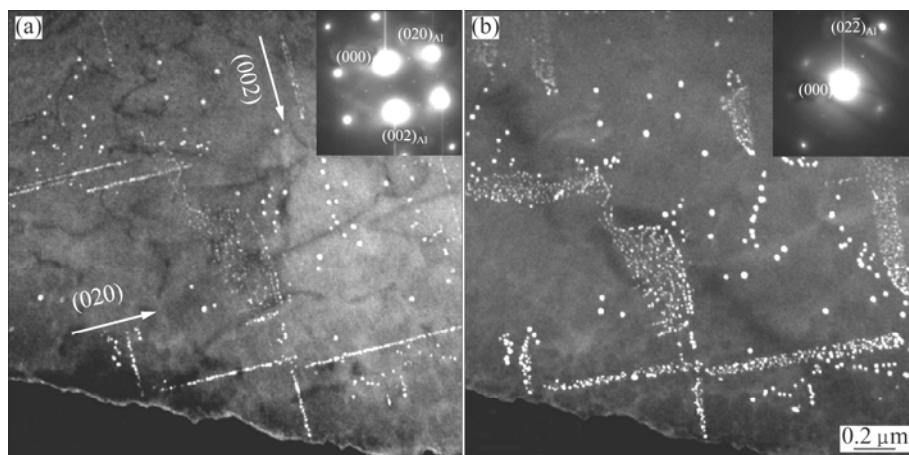
Fig. 3 Oriented precipitations of Al$_3$Zr precipitates along {100} Al planes: (a) TEM dark-field image taken from [100] zone axis; (b) Dark-field image from same area as (a) but after 30° tilting (The sample is the Al−Cu-Zr alloy heat treated at 500 °C for 1 h)

In order to check stability of the Al$_3$Zr precipitate, the sample of the Al−Cu−Zr alloy was heat treated for a long time, i.e. 20 h at 500 °C, and subsequently investigated by TEM. Figure 4 shows precipitates at dendrite edge. Some of precipitates show dark contrast lines in the middle (Fig. 4(a)), which is interpreted as anti-phase boundaries (APB) [11], indicating the phase transformation from metastable L1$_2$ to D0$_{23}$ structure. High magnification images of the precipitate display an ellipsoidal shape with a long axis along the anti-phase boundary (APB) (Fig. 4(b)) and plane faults in the APB are revealed.
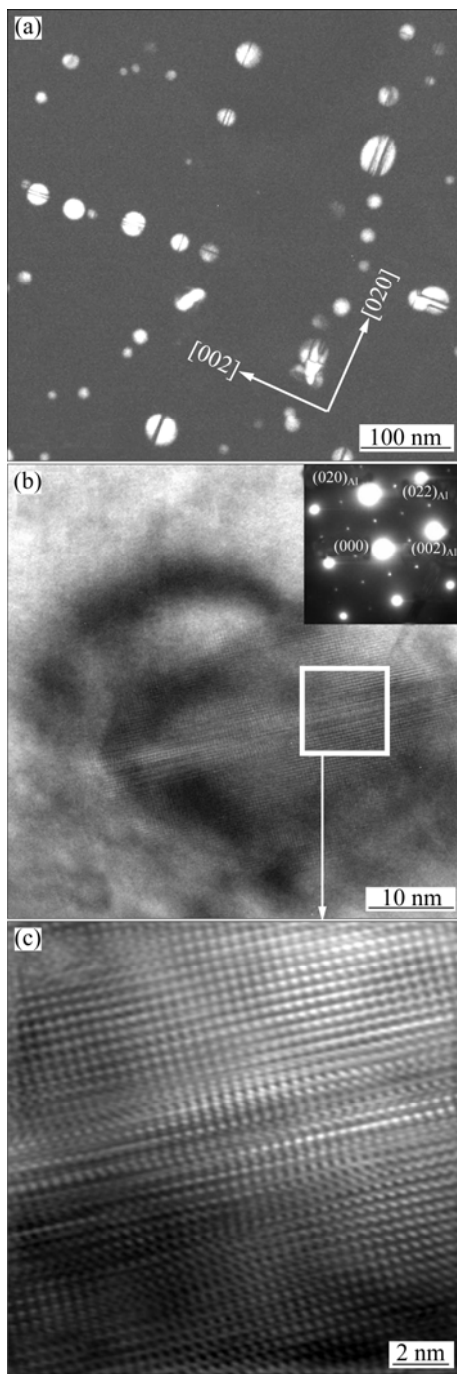
Fig. 4 TEM images of Al−Cu−Zr alloy heat treated at 500 °C for 20 h showing APBs on some large Al$_3$Zr precipitates: (a) Low magnification dark-field image showing precipitates with no contrast lines along two perpendicular orientations; (b, c) High-resolution images of one precipitate showing planar faults

4 Discussion

TEM investigations reveal homogeneous distribution of coherent Al$_3$Zr precipitates in dendrite centres, but inhomogeneous distribution at dendrite edges and in interdendritic regions (Fig. 1).

Microsegregation of Zr in the Al solid solution during solidification was studied previously [12]. Compositional analysis of a dendrite by line scan on an electron microprobe confirmed the Zr microsegregation to the dendrite centres in the present Al−Cu based alloys, which results in different driving forces for nucleation and growth of Al$_3$Zr precipitate from dendrite centre to the edges. Higher solution temperatures like 540 °C to reduce microsegregation of Zr did not improve the distribution but coarsened the Al$_3$(Zr,Ti,V) precipitates in the dendrite centre. Homogeneously distributed spherical Al$_3$(Zr,Ti,V) precipitates in dendrite centres originated from a high supersaturation of Zr. However, with a decrease of the Zr level close to dendrite edges or interdendritic regions, the nucleation and growth of Al$_3$(Zr,Ti,V) precipitates are limited by a lower driving force. The nucleation is often related to dislocations or pre-existing particles, which can lower the energy barrier for nucleation.

The mean radius of the Al$_3$(Zr,Ti,V) precipitate of 5.8 nm is comparable with measurements for Al−Zr−Ti alloy [11]. Addition of Ti is confirmed not to influence the size of the Al$_3$Zr precipitate although it substitutes Zr partly in the precipitates [12]. Addition of V is shown to reduce the coarsening rate of Al$_3$Zr precipitate but does not seem to affect the size of the Al$_3$Zr precipitates [21−23]. It is well established that nucleation and precipitation of the Al$_3$Zr precipitate strongly depend on supersatuation of Zr in the Al solid solution at a given temperature and thus determine the precipitate size and density. Addition of Cu can reduce the metastable Zr solubility [13,24] and its effect increases with increasing Cu content [13]. Although the added Zr amount (0.2%) in the present alloy is lower than that (0.34%) in the Al−Zr−Ti alloy [11], a similar supersaturation of Zr is reached by the addition of Cu. In addition, the slow heating rate of 50 °C/h applied to the present alloys compared with 3 h isochronal aging in Al−Zr−Ti alloy [11] also has a certain contribution to a smaller radius of the Al$_3$Zr precipitate [14].

Different precipitation behaviours lead to variation of the precipitate size and morphology. KNIPLING et al [12] observed cauliflower-shaped, rod-like and plate-like L1$_2$ Al$_3$(Zr,Ti) precipitates in interdendritic regions oriented along ⟨100⟩-type matrix directions and a close-up of the rod-like precipitates revealed the rod pairs with spacing of ~10 nm. Observations of interdendritic regions in the present alloys showed helical-like and stripe-like precipitation. Both shapes are composed of many small Al$_3$(Zr,Ti,V) precipitates. Dislocations were observed to be related to some of the helical rims with a large size of precipitates (Fig. 2). However, comparison from dark-field images (Figs. 2(b) and (d)) in stripe-shaped precipitates indicates that the

stripe-like precipitates are not completely related to dislocations. Another characteristic feature of many stripe-like precipitates is preferentially arranged along {100} Al planes, as confirmed by tilting experiments (Fig. 3). This is observed for the first time and different from the earlier reported results [12]. ROBSON et al [6] observed elongated clusters composed of spherical precipitates. There seem to be some similarities to what we observed here, such as, precipitate length and orientation. However, elongated clusters are only observed in one direction which was not indicated here.

The strip-like morphologies display regular or irregular shapes (Fig. 3(b)). It is clear that these oriented precipitation clusters do not originate from dislocations, but they are most likely related to Al_2Cu precipitates. The studied alloy includes 5% Cu. During heating to 500 °C all stages of Al_2Cu precipitates occur. The θ'-Al_2Cu phase which has an orientation relationship with the $\langle 100 \rangle$ Al matrix is observed over 300 °C and the complete phase transformation to the θ stable phase can last a long time, varying from one alloy to another [25]. In the case, Zr in the interdendritic regions may preferentially diffuse and nucleate at Al_2Cu sites which will be dissolved into the Al solid solution at a higher temperature. Oriented precipitation clusters were not observed in dendrite centres because homogeneous precipitation is dominant due to high supersaturation of Zr.

Precipitation evolution of Al_3Zr from metastable $L1_2$ to stable $D0_{23}$ structure was also investigated from the sample heat treated at 500 °C for 20 h (Fig. 4). Metastable $L1_2$ Al_3Zr precipitates show dark contrast lines or bands across the precipitate centres which are explained as APB, indicating the initiation of the transformation to equilibrium $D0_{23}$ structure. DAHL et al [26] investigated several Al−Zr alloys containing 0.03%−0.36% Zr aged at 200−500 °C and concluded that the $L1_2 \rightarrow D0_{23}$ structural transformation began after several hundred hours at 500 °C. KNIPLING et al [11] observed similar precipitation evolution in Al−Zr−Ti alloy after peak aging at 375 °C for 100 h followed by precipitation aging at 500 °C for 100 h. Addition of Cu in the present alloy seems to promote the $L1_2 \rightarrow D0_{23}$ structural transformation of the Al_3Zr precipitate. HRTEM images reveal that $L1_2$ Al_3Zr precipitate is elongated along the direction of APBs.

5 Conclusions

1) Homogeneously distributed coherent Al_3Zr precipitates with high density were observed in dendrite centres.

2) Helical-like and stripe-like clusters composed of precipitates were observed at interdendritic regions.

3) The clusters have a preferentially orientation relationship with the $\langle 100 \rangle$ Al directions, which are inferred to be related to θ'-Al_2Cu and θ phases. Addition of Cu can accelerate the $L1_2 \rightarrow D0_{23}$ structural transformation of the Al_3Zr precipitate.

References

[1] GAYLE F W, GOODWAY M. Precipitation hardening in the first aerospace aluminum alloy—The wright flyer crankcase [J]. Science, 1994, 266(5187): 1015−1017.

[2] RINGER S P, HONO K. Microstructural evolution and age hardening in aluminium alloys: Atom probe field-ion microscopy and transmission electron microscopy studies [J]. Materials Characterization, 2000, 44(1−2): 101−131.

[3] CLOUET E, SANCHEZ J M, SIGLI C. First-principles study of the solubility of Zr in Al [J]. Phys Rev B, 2002, 65(9): 094105.

[4] RYUM N. Precipitation and recrystallization in an Al−0.5 wt percent Zr-alloy [J]. Acta Metall, 1969, 17(3): 269−278.

[5] CLOUET E, NASTAR M, SIGLI C. Nucleation of Al_3Zr and Al_3Sc in aluminum alloys: From kinetic Monte Carlo simulations to classical theory [J]. Phys Rev B, 2004, 69(6): 064109.

[6] ROBSON J D, PRANGNELL P B. Dispersoid precipitation and process modelling in zirconium containing commercial aluminium alloys [J]. Acta Mater, 2001, 49(4): 599−613.

[7] NES E, BILLDAL H. Mechanism of discontinuous precipitation of metastable Al_3Zr phase from an Al−Zr solid-solution [J]. Acta Metall, 1977, 25(9): 1039−1046.

[8] ROBSON J D, JONES M J, PRANGNELL P B. Extension of the N-model to predict competing homogeneous and heterogeneous precipitation in Al−Sc alloys [J]. Acta Mater, 2003, 51(5): 1453−1468.

[9] KNIPLING K E, DUNAND D C, SEIDMAN D N. Atom probe tomographic studies of precipitation in Al−0.1Zr−0.1Ti (at.%) alloys [J]. Microsc Microanal, 2007, 13(6): 503−516.

[10] KNIPLING K E, DUNAND D C, SEIDMAN D N. Nucleation and precipitation strengthening in dilute Al−Ti and Al−Zr alloys [J]. Metall Mater Trans A, 2007, 38(10): 2552−2563.

[11] KNIPLING K E, DUNAND D C, SEIDMAN D N. Precipitation evolution in Al−Zr and Al−Zr−Ti alloys during aging at 450−600 °C [J]. Acta Mater, 2008, 56(6): 1182−1195.

[12] KNIPLING K E, DUNAND D C, SEIDMAN D N. Precipitation evolution in Al−Zr and Al−Zr−Ti alloys during isothermal aging at 375−425 °C [J]. Acta Mater, 2008, 56(1): 114−127.

[13] ROBSON J D, PRANGNELL P B. Modelling Al_3Zr dispersoid precipitation in multicomponent aluminium alloys [J]. Mater Sci Eng A, 2003, 352(1−2): 240−250.

[14] SATO T, KAMIO A, LORIMER G W. Effects of Si and Ti additions on the nucleation and phase stability of the $L1_2$-type Al_3Zr phase in Al−Zr alloys [C]// The 5th International Conference on Aluminium Alloys. Grenoble, France: Trans Tech Publications, 1996: 895−900.

[15] HAN S Z, PARK S I, HUH J S, LEE Z H, LEE H M. Lattice matching of D0(23) and D0(22) phases in Al−6at%(Ti, V, Zr) systems [J]. Mater Sci Eng A, 1997, 230(1−2): 100−106.

[16] FORBORD B, HALLEM H, MARTHINSEN K. The effect of alloying elements on precipitation and recrystallization in Al−Zr alloys [C]// The 9th International Conference on Aluminium Alloys. Brisbane, Australia: Institute of Materials Engineering Australasia

Ltd, 2004: 1179−1185.

[17] FORBORD B, HALLEM H, RYUM N, MARTHINSEN K. Precipitation and recrystallisation in Al−Mn−Zr with and without Sc [J]. Mater Sci Eng A, 2004, 387−389: 936−939.

[18] JIA Z H, HU G Q, FORBORD B, SOLBERG J K. Effect of homogenization and alloying elements on recrystallization resistance of Al−Zr−Mn alloys [J]. Mater Sci Eng A, 2007, 444: 284−290.

[19] RIDDLE Y W, SANDERS T H. Recrystallization performance of AA7050 varied with Sc and Zr [J]. Mater Sci Forum, 2000, 331−337: 799−804.

[20] SEPEHRBAND P, MAHMUDI R, KHOMAMIZADCH F. Effect of Zr addition on the aging behavior of A319 aluminum cast alloy [J]. Scripta Mater, 2005, 52: 253−257.

[21] CHEN Y C, FINE M E, WEERTMAN J R. Microstructural evolution and mechanical properties of rapidly solidified Al−Zr−V alloys at high-temperatures [J]. Acta Metall Mater, 1990, 38: 771−780.

[22] CHEN Y C, FINE M E, WEERTMAN J R, LEWIS R E. Coarsening behavior of Ll$_2$ Structured Al$_3$(Zr$_x$V$_{1−x}$) precipitates in rapidly solidified Al−Zr−V alloy [J]. Scripta Metall 1987, 21(7): 1003−1008.

[23] ZEDALIS M S, FINE M E. Precipitation and Ostwald ripening in dilute Al base−Zr−V alloys [J]. Metall Trans A, 1986, 17(12): 2187−2198.

[24] SIGLI C. Zirconium solubility in aluminium alloys [C]// The 9th International Conference on Aluminium Alloys. Brisbane, Australia: Institute of Materials Engineering Australasia Ltd, 2004: 1353−1358.

[25] CHERDOUDI N, COUZINIE J P, GUILLOT I, LEROY E, BARLAS B, MASSINON D. Influence of silicon and residual elements on the precipitation of cast aluminium-copper alloy [C]//The 11th International Conference on Aluminium Alloys. Aachen, Germany: Wiley-VCH, 2008: 969−974.

[26] DAHL W, GRUHL W, BURCHARD G W, IBE G, DUMITRESCU C. Solidification and precipitation in aluminum-zirconium alloys (2): Precipitation processes in cast aluminum-zirconium alloys [J]. Zeit Metallkd, 1977, 68(3): 188−194.

Al−Cu−Zr 和 Al−Cu−Zr−Ti−V 合金中 Al$_3$Zr 析出相的析出行为

贾志宏 [1,2], Jean-Philippe COUZINIÉ [3], Nadia CHERDOUDI [3], Ivan GUILLOT [3], Lars ARNBERG [2],

Petter ÅSHOLT [4], Stig BRUSETHAUG [4], Bruno BARLAS [5], Denis MASSINON [5]

1. 重庆大学 材料科学与工程学院，重庆 400044;

2. Department of Materials Science and Engineering, Norwegian University of Science and Technology,

NO-7491, Trondheim, Norway;

3. Institut de Chimie et des Matériaux Paris-Est, UMR 7182 CNRS-Unversité Paris Val de Marne,

2-8 rue Henri Dunant, 94320 Thiais, France;

4. Hydro Aluminium Research and Technology Development, N-6601 Sunndalsøra,

Norway Montupet SA, 60181 Nogent sur Oise Cedex, France;

5. Mentupet SA, 60181 Nogent sur Oise Cedex, France

摘 要: 利用透射电子显微技术研究 Al−Cu−Zr 和 Al−Cu−Zr−Ti −V 合金中 Al$_3$Zr 的沉淀析出行为。亚稳态的 Al$_3$Zr 沉淀相在枝晶中心均匀形核并获得均匀分布。然而，在枝晶边缘区域的析出复杂，观察到由许多球形 Al$_3$Zr 析出颗粒组成的螺旋状和条状的形貌。条状的沉淀团簇沿⟨100⟩铝方向优先排列，这可能与 Al$_2$Cu 的亚稳态 θ' 和稳态 θ 析出相相关。添加铜有利于 Al$_3$Zr 沉淀相从 L1$_2$→D0$_{23}$ 的结构转变。

关键词：铝合金；Al$_3$Zr 析出相；相转变

(Edited by LI Xiang-qun)